

## Supporting Information for

# Highly Efficiency Coupled Electrocatalytic CO<sub>2</sub> Reduction to C<sub>2</sub>H<sub>4</sub> with 5-Hydroxymethylfurfural Oxidation over Cu-based Nanoflower electrocatalyst

Zonghang Zhang,<sup>a</sup> Shan Liu,<sup>a</sup> Zhao Wu,<sup>b\*</sup> Xiaoyan Chen,<sup>a</sup> Jingui Wang,<sup>a</sup> Yuji Gao,<sup>a</sup>

Shuai Wang,<sup>a</sup> Furong Tao,<sup>a</sup> Guangqiang Lv,<sup>a\*</sup>

<sup>a</sup> *Shandong Provincial Key Laboratory of Molecular Engineering, Qilu University of Technology (Shandong Academy of Sciences), Jinan 250353, Shandong, China;*

<sup>b</sup> *Safety and environmental protection department of Sinopec Jinan Company, Jinan, Shandong 250101;*

Corresponding Authors:

Guangqiang Lv: E-mail: [lvguangqiang@qlu.edu.cn](mailto:lvguangqiang@qlu.edu.cn);

Zhao Wu: E-mail: [wuzhao.jnlh@sinopec.com](mailto:wuzhao.jnlh@sinopec.com)

- 1. Chemicals**
- 2. Materials synthesis**
- 3. Characterization**
- 4. Electrocatalysis experiments**
- 5. Product analysis**
- 6. Calculation of product FE and yield**

## 1. Chemicals

Ammonium persulfate  $(\text{NH}_4)_2\text{S}_2\text{O}_8$  (99.0%, AR, grade), potassium hydroxide was bought from Macklin. Dimethyl sulfoxide (DMSO) and deuterium water ( $\text{D}_2\text{O}$ ) were bought from Aladdin. Methanol, ethanol, hydrochloric were bought from Tianjing FUYU. Copper foam was bought from Shenzhen KEJING. Carbon cloth、FAA-3-PK130 membrane and N117 membrane was bought from Suzhou SHENGNUO. All chemicals were used as received without any further purification. Deionized water (DIW) was used in all experiments.

## 2. Materials synthesis

Ultra-thin nanosheets were grown on foam copper using an in-situ method. First, the foam copper ( $1\text{cm} \times 1\text{cm} \times 1\text{mm}$ ) was sequentially washed in acetone, hydrochloric acid, and anhydrous ethanol for 30 minutes each. Then, 22 g sodium hydroxide was dissolved in 100mL of deionized water, followed by the addition of 4.5 g  $(\text{NH}_4)_2\text{S}_2\text{O}_8$ . The solution was heated to  $70^\circ\text{C}$  with magnetic stirring until all  $(\text{NH}_4)_2\text{S}_2\text{O}_8$  was dissolved. The cleaned foam copper was fully immersed in the solution, and after 10 minutes of reaction, the color of the foam copper changed from golden to blue, resulting in  $\text{Cu}(\text{OH})_2$  nanorod catalyst. After 20 minutes of reaction, a deep blue  $\text{CuO}/\text{Cu}(\text{OH})_2$  catalyst was obtained, which turned into black  $\text{CuO}$  ultra-thin nanosheet catalyst upon stirring. The prepared catalysts were washed three times with water and ethanol, and soaked in deionized water for 6 hours. Finally, the catalysts were dried overnight in a drying oven at  $60^\circ\text{C}$ .

For the Cu<sub>2</sub>O/Cu-NF@GDL catalyst used in the flow cell, The preparation of the cathodic Cu<sub>2</sub>O/Cu-NF@GDL was as follows. The CuO-NF@Cu catalyst was subjected to blade scraping to remove the black CuO-NF on its surface, resulting in CuO-NF powder. The powder, weighing 5 mg, was dissolved in 1 mL acetone and mixed with 20 uL of Nafion solution. Next, 510 uL of the solution was uniformly spread onto a 1×1 cm<sup>2</sup> carbon cloth and dried at room temperature. The CuO-NF loading on the carbon cloth was 2.5 mg/cm<sup>2</sup>. The Cu<sub>2</sub>O/Cu-NF@GDL catalyst is obtained through electroreduction of CuO-NF@GDL.

### **3. Characterization**

Materials Characterization: Power X-ray diffraction (XRD) patterns were collected on a Rigaku MiniFlex II desktop X-ray diffractometer using Cu K $\alpha$  radiation at 40 kV and 40 mA with a scanning speed ( $2\theta$ ) of 3 °/min. Scanning Electron Microscopy (SEM) was measured on a JSM-7001F microscope. TEM (Transmission electron microscope) was conducted on a JEM-2100F microscope. AFM (Atomic Force Microscopy) was measured on a Multimode8. A small amount of copper foam was sonicated in ethanol solution for 5 min, and then the solution was added dropwise to the copper mesh and fluorine mica flakes and tested with TEM and AFM, respectively. X-ray photoelectron spectroscopy (XPS) measurements were performed by a K-alpha XPS spectrometer using monochromatic Al K $\alpha$  radiation generated from an electron beam operated at 15 kV and 32.3 W. Samples were collected under ultra-high vacuum (at 10<sup>-7</sup> mbar) and room temperature at a pass energy of 50 eV to avoid sample charging. In order to compensate for the charging effect, all binding energies were referenced to

the C 1s of 288.2 eV. The depth of focus distribution was recorded by alternating cycles of XPS analysis and sputtering, focusing a 1 kV Ar<sup>+</sup> ion beam on a surface area of 50 μm diameter. The peak fitting was carried out by the Avantage (Thermo Scientific) software package. Inductively coupled plasma optical emission spectrometry (ICP-OES) analysis was recorded on Agilent 700 Series instrument.

#### **4. Electrocatalysis experiments**

All the electrochemical experiments were conducted on the electrochemical workstation (CHI 760E, Shanghai CH Instruments Co., China). An airtight electrolytic hydrogen cell, separated by a Nafion 117 membrane, was used to measure the CO<sub>2</sub>RR performance of the catalyst. The cathode and anode electrolytes were both 15 mL of 0.5 M KCl. Prior to the CO<sub>2</sub>RR experiment, ultra-pure carbon dioxide gas was continuously bubbled into the cathode electrolyte for 30 minutes to saturate the solution with carbon dioxide, while the anode electrolyte was bubbled with ultra-pure argon for 30 minutes. Platinum foil (1×1 cm<sup>2</sup>) and an Ag/AgCl electrode saturated with KCl solution were used for the working and reference electrodes, respectively. During the CO<sub>2</sub>RR, the flow rate of carbon dioxide was kept at 15 sccm and the stirring speed of the catholyte was maintained at 700 rpm. In the long-term CO<sub>2</sub>RR stability test, the CO<sub>2</sub>-saturated KCl electrolyte was replaced every 10 hours, and at each applied potential, 1 hour of electrolysis was performed using the CHI 760E potentiostat, and the faradaic efficiency of each product was measured. All applied potentials were converted to the RHE by the equation: E (vs RHE)

= E (vs Ag/AgCl) +0.204 V + 0.0591 V × pH, No iR compensation. Prior to use, the concentrations of the 5 standard gases (H<sub>2</sub>, CO, CH<sub>4</sub>, C<sub>2</sub>H<sub>2</sub>, C<sub>2</sub>H<sub>4</sub> and C<sub>2</sub>H<sub>6</sub> in CO<sub>2</sub>) were corrected by a concentration gradient at a flow rate of 15 mL/min. The gas sample was analyzed after at least 30 minutes of electrolysis to ensure the CO<sub>2</sub>RR reached a steady state. After 1 hour of electrolysis, liquid samples were collected and analyzed by nuclear magnetic resonance spectroscopy using dimethyl sulfoxide (DMSO) as an internal standard.

A three-electrode cell consisting of a prepared working electrode (geometric area of 1 cm<sup>2</sup>), a graphite rod counter electrode, and an Ag/AgCl (4 M KCl) reference electrode was employed for the constant potential oxidation of HMF. The cell was used in an H-shaped divided cell with a proton exchange membrane (N117) as the separator. The electrolyte in the working electrode (anode) compartment was a 20 mL 0.1 M potassium hydroxide (pH 13) solution containing 10 mM HMF. The electrolyte in the counter electrode (cathode) compartment was a 20 mL 0.1 M potassium hydroxide (pH 13) solution. The electrochemical oxidation was carried out at room temperature with continuous stirring of the solution at a rate of 400 rpm. A specific voltage of 1.62 V (vs RHE) was applied to pass a charge of 116 C (the coulombic efficiency required for the conversion of the given amount of HMF to FDCA is 115.6 C).

For the electrochemical CO<sub>2</sub>RR-HMFOR testing in a flow cell, a commercial flow cell electrolysis cell with an effective area of 1 cm<sup>2</sup> was used. The Cu<sub>2</sub>O/Cu-NF@GDL was used as the cathode, and the catholyte was

10 mL/min KCl (1 M). The CuO-NF@Cu was used as the anode, and the anolyte was composed of a 5 mL/min HMF solution (10 mM) and a 5 mL/min KOH solution (2 M), which was mixed through a tee during the reaction to prevent HMF polymerization under strong alkaline conditions. The cathode and anode chambers were separated by a bipolar membrane (BPM) during the reaction. Atypical BPM consists of laminated films of anion-exchange layer (AEL) and cation-exchange layer (CEL) with a bipolar interfacial layer (IL) formed between that allows selective diffusion of protons and hydroxide anions towards the negative and positive electrode, respectively. During the CO<sub>2</sub>RR process, the gas flow rate was set to 15 mL/min. The catholyte and anolyte were circulated at speeds of 10 mL/min, respectively, using a peristaltic pump.

## 5. Product analysis

After electrolysis reaction, For carbon dioxide reduction reaction, the gaseous products were tested online and then analyzed by an Agilent 4890 gas chromatograph equipped with an TCD (Porapak-S 80/100mesh 3.2mm\*2.0mm\*3M and MS-13X 80/100mesh 3.2mm\*2.0mm\*3M) and FID detector (Rtx-1 0.53mm\*5.0um\*30m). The cathode liquid products were analyzed by <sup>1</sup>H NMR measured on a Bruker Avance III 400 HD spectrometer. The Faradaic efficiency of the cathode products was calculated through GC and NMR analysis.

For HMF oxidation, during and after the reaction, 150  $\mu$ L of the solution was extracted from the anode chamber and analyzed by HPLC using a SY-9100 system (HPLC with an Aminex HPX-87H column from Bio-Rad

Laboratories Co., Ltd., with 0.5 mM H<sub>2</sub>SO<sub>4</sub> aqueous solution as the eluent, a flow rate of 0.6 mL/min, and a temperature of 35°C) to calculate the conversion and yield of HMF oxidation products.

## 6. Calculation of product FE, selectivity and yield

Cathode: After the quantification, the FE of each product was calculated as follows:

$$FE(\%) = \frac{Q_x \times n_x N_x \times F}{Q_{total} \times t \times F} \times 100\%$$

where Q<sub>x</sub> and Q<sub>total</sub> was the charge passed into product x and totally passed charge(C) during CO<sub>2</sub>RR, n<sub>x</sub> represents the electron transfer number of product x, N<sub>x</sub> was the product amount (mol) of x measured by GC or NMR and F was the Faradayconstant (96485 C mol<sup>-1</sup>).

Product selectivity of C<sub>2</sub>H<sub>4</sub> (%) =

$$\frac{n(C_2H_4)}{n(C_2H_4) + n(CO) + n(CH_4) + n(HCOOH) + n(C_2H_5OH) + n(CH_3COOH)} \times 100\%$$

where n(C<sub>2</sub>H<sub>4</sub>), n(CO), n(CH<sub>4</sub>), n(HCOOH), n(C<sub>2</sub>H<sub>5</sub>OH), n(CH<sub>3</sub>COOH) and n(CO) are the amounts of produced C<sub>2</sub>H<sub>4</sub>, CO, CH<sub>4</sub>, HCOOH, C<sub>2</sub>H<sub>5</sub>OH, CH<sub>3</sub>COOH and CO.

Anode: After the quantification, the conversion of HMF and the yield of each product were calculated as follows:

$$\begin{aligned}
 & \text{HMF conversion (\%)} = \frac{\text{m o l o f H M F}}{\text{m o l o f i n i t i a l H M F}} \times 100\% \\
 & \text{yield of product(\%)} = \frac{\text{m o l o f p r o d u c t}}{\text{m o l o f i n i t i a l H M F}} \times 100\% \\
 & \text{FE(\%)} \text{ for FDCA production} = \frac{\text{m o l o f p r o d u c t}}{\text{m o l o f t o t a l e l e x c t r o n s}} \times 100\%
 \end{aligned}$$

100%

Product selectivity of FDCA (\%) =

$$\frac{n(F D C A)}{n(H M F) + n(D F F) + n(F F C A) + n(F D C A)} \times 100\%$$

where  $n(\text{HMFCA})$ ,  $n(\text{DFF})$ ,  $n(\text{FFCA})$  and  $n(\text{FDCA})$  are the amounts of produced HMFCA, DFF, FFCA and FDCA.

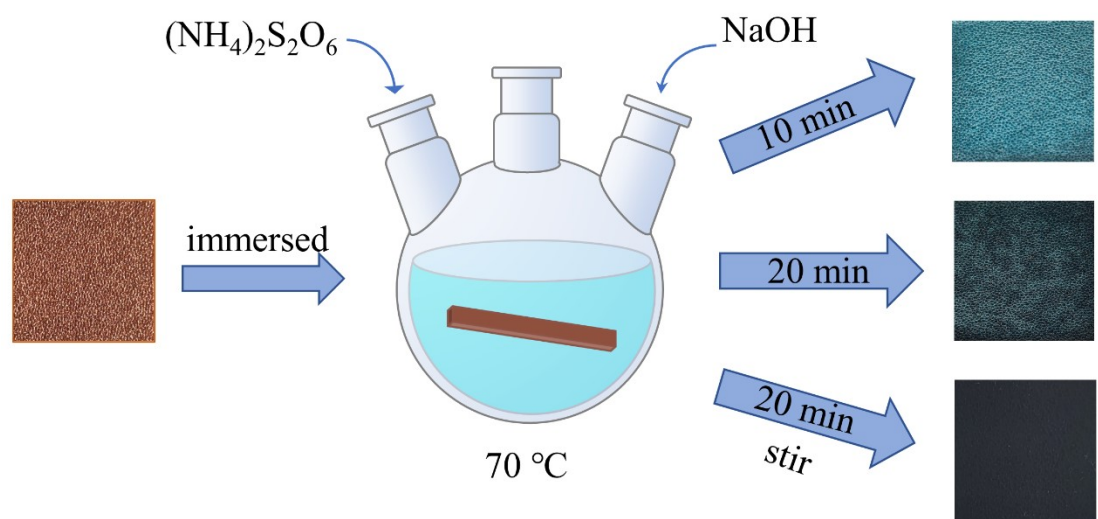


**Figure S1.** Schematic diagram for the synthesis of catalyst and photo-image of Cu foam under different conditions

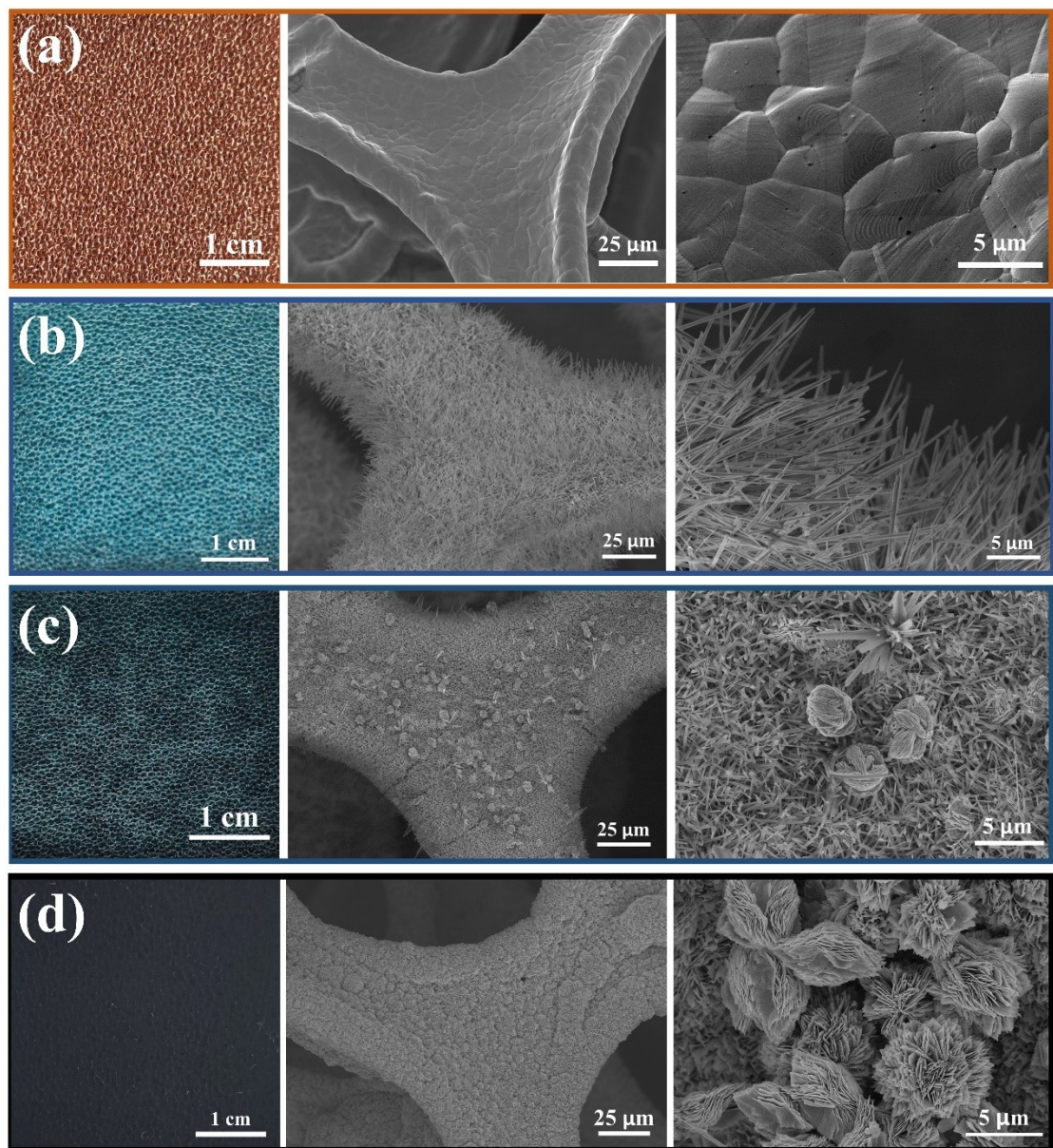


**Figure S2.** SEM images of (a) Cu foam, (b) Cu(OH)<sub>2</sub> -NR@Cu, (c) CuO/Cu(OH)<sub>2</sub>@Cu, and (d) CuO-NF@Cu

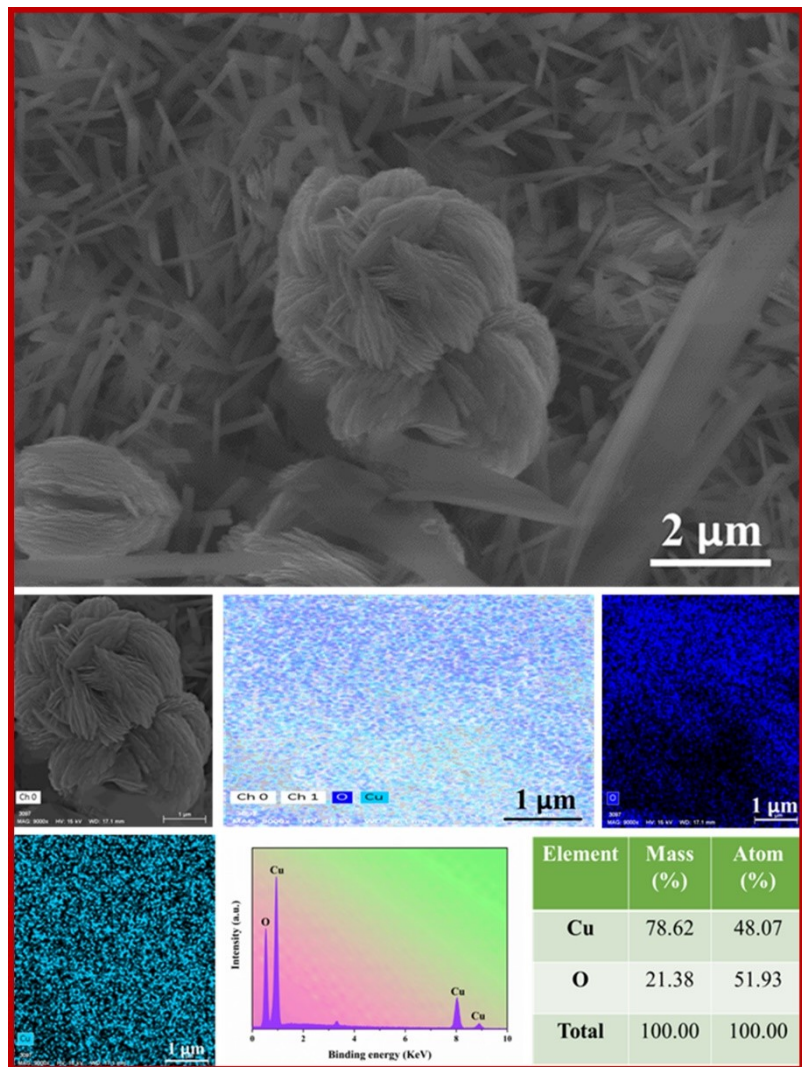


**Figure S3.** SEM images and elemental mapping images EDS spectrum of CuO/Cu(OH)<sub>2</sub>@Cu

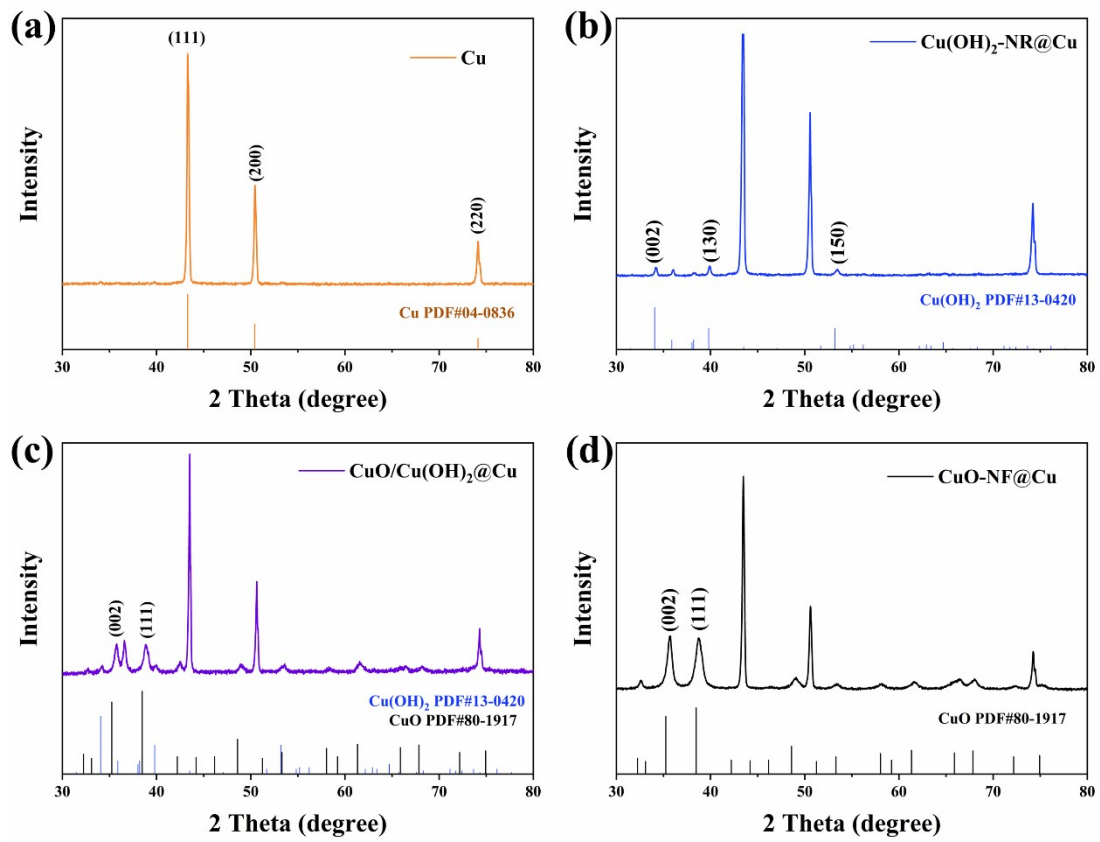


**Figure S4.** XRD patterns of (a) Cu foam, (b) Cu(OH)<sub>2</sub>-NR@Cu, (c) CuO/Cu(OH)<sub>2</sub>@Cu and (d) CuO-NF@Cu

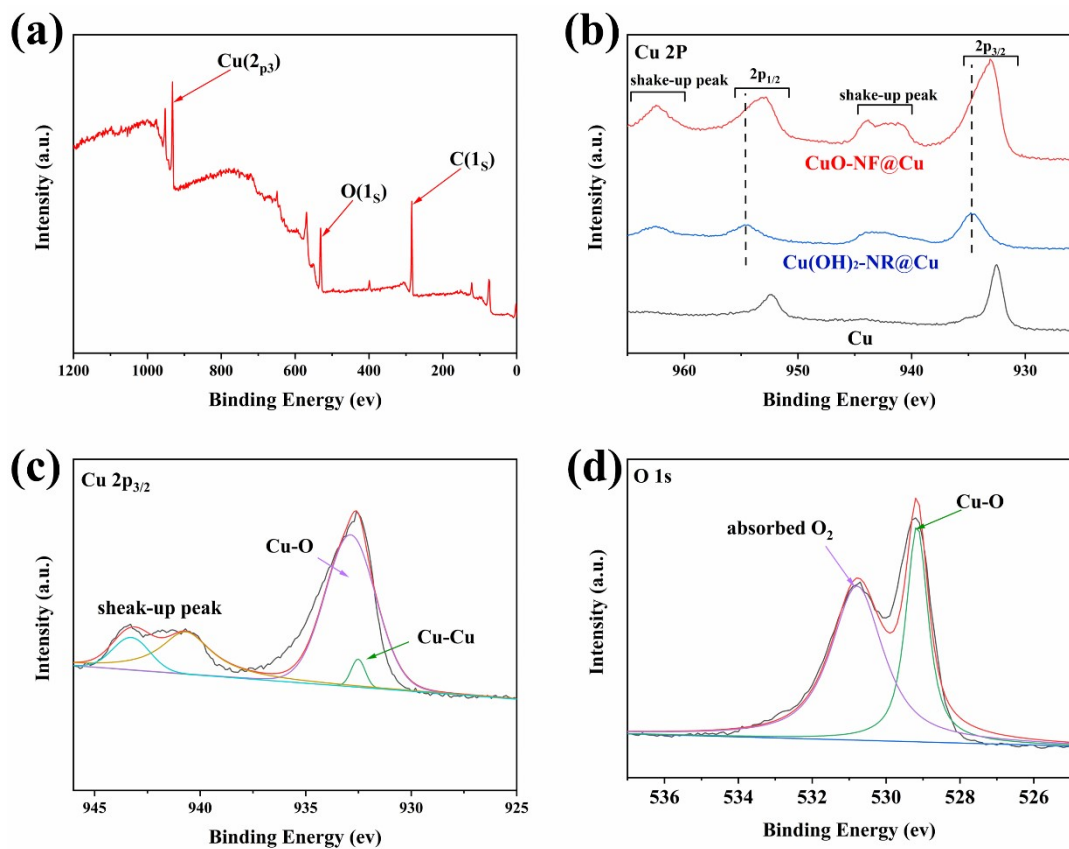


**Figure S5.** (a) XPS survey spectrum of CuO-NF@Cu, (b) High resolution Cu 2P XPS spectra of CuO-NF@Cu and comparison with Cu(OH)<sub>2</sub>-NR@Cu and Cu foam, (c) High resolution Cu 2p<sub>3/2</sub> spectrum of obtained CuO nanosheets on Cu foam. (d) High resolution O 1s XPS spectra of CuO-NF@Cu

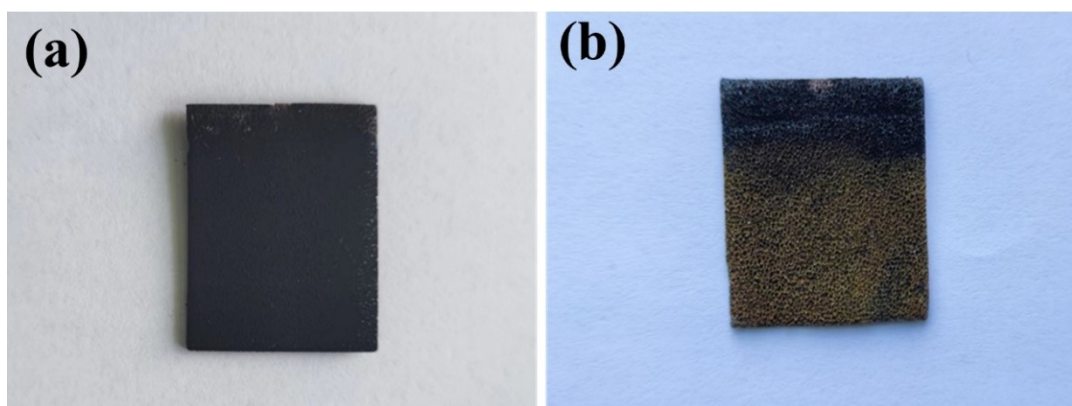


**Figure S6.** Optical images of fresh CuO-NF@Cu and reduced Cu<sub>2</sub>O/Cu-NF@Cu after 5 min electrolysis at -0.95 V (vs RHE)

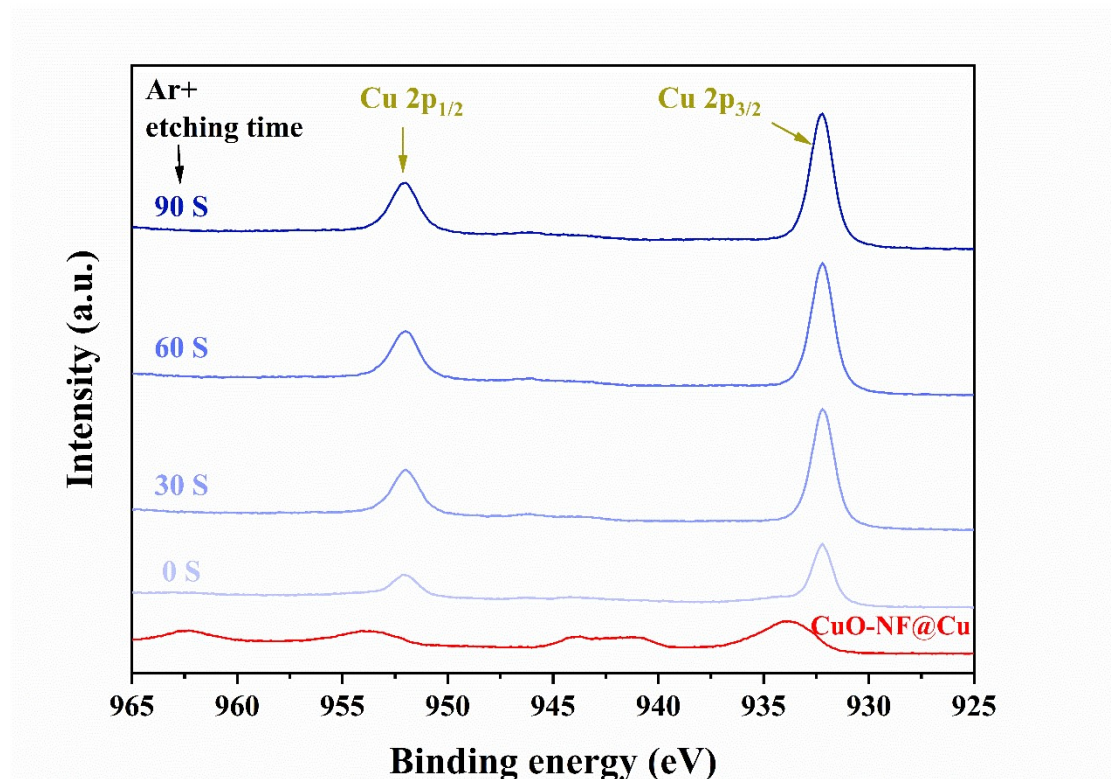


**Figure S7.** Cu XPS 2p spectra of CuO-NF@Cu and Cu<sub>2</sub>O/Cu-NF@Cu (2 h reduction)

with different Ar<sup>+</sup> etching time. The Cu<sub>2</sub>O/Cu-NF@Cu sample taken after CO<sub>2</sub>RR shows consistent Cu<sup>0</sup>/Cu<sup>+</sup> 2p peaks, Cu peaks intensities increase as the etching time extended, due to the increase content of the Cu element in the deeper subsurface with Ar<sup>+</sup> etching time increasing

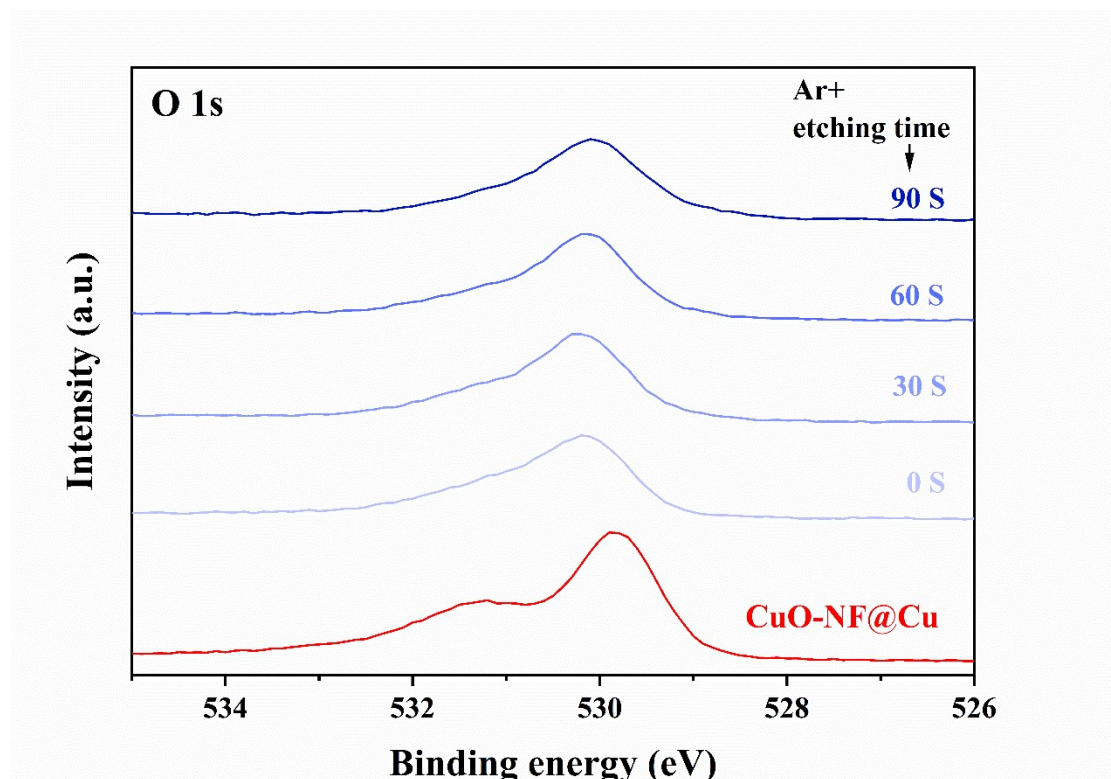


**Figure S8.** O XPS 1s spectra of CuO-NF@Cu and Cu<sub>2</sub>O/Cu-NF@Cu (2 h reduction)

with different Ar<sup>+</sup> etching time. The peaks located at 529.9 eV (CuO-NF@Cu) and 530.5 eV (Cu<sub>2</sub>O/Cu-NF@Cu) could be ascribed to CuO and Cu<sub>2</sub>O, respectively. The peak intensities of O decrease as the etching time extended, due to the detection of deeper subsurface with Ar<sup>+</sup> etching time increasing

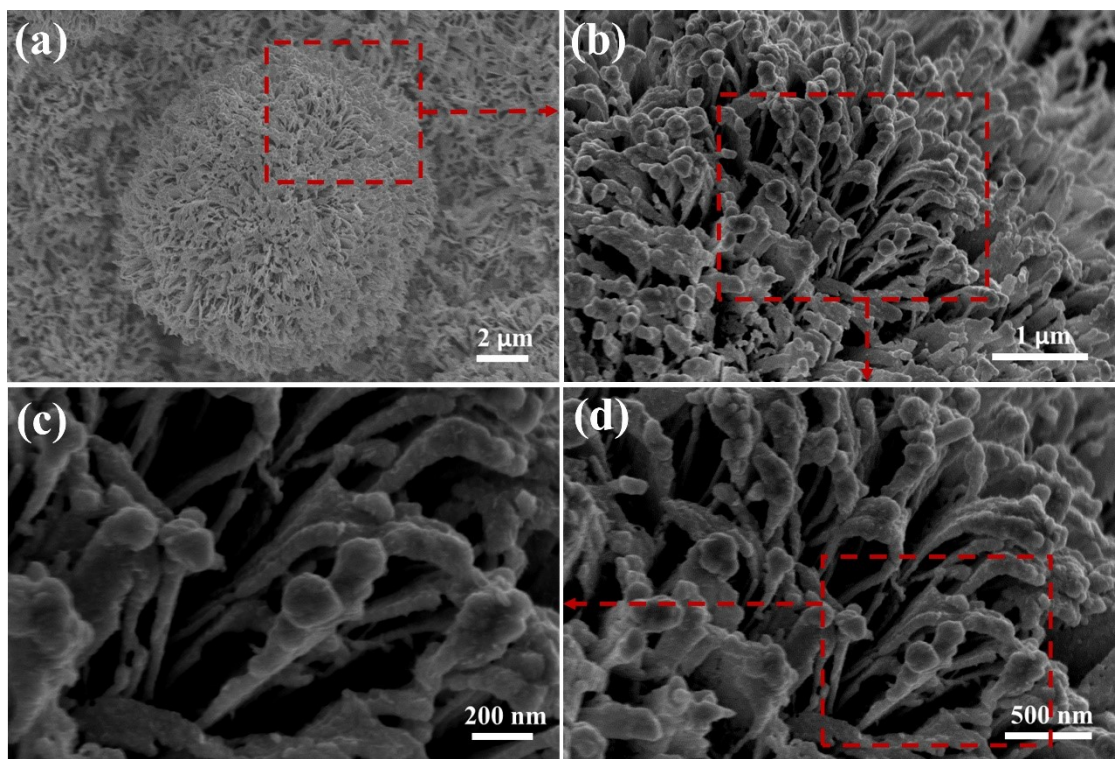


**Figure S9.** SEM images of Cu<sub>2</sub>O/Cu-NF@Cu

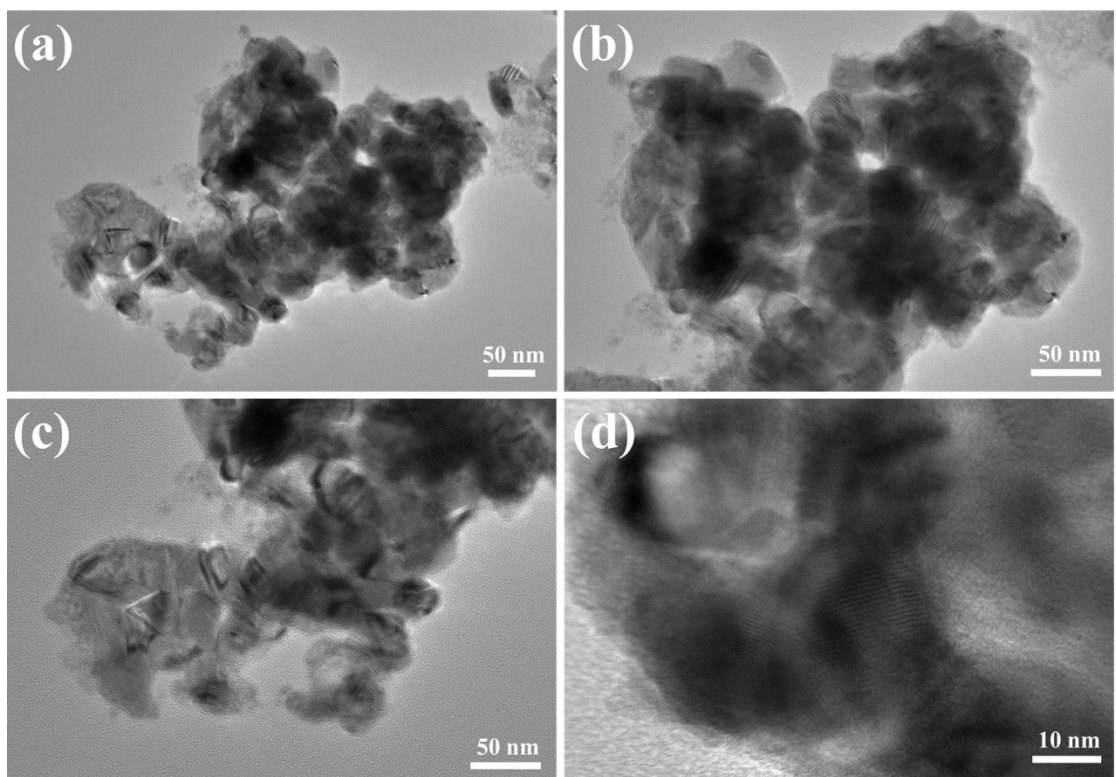


**Figure S10.** TEM images of Cu<sub>2</sub>O/Cu-NF@Cu

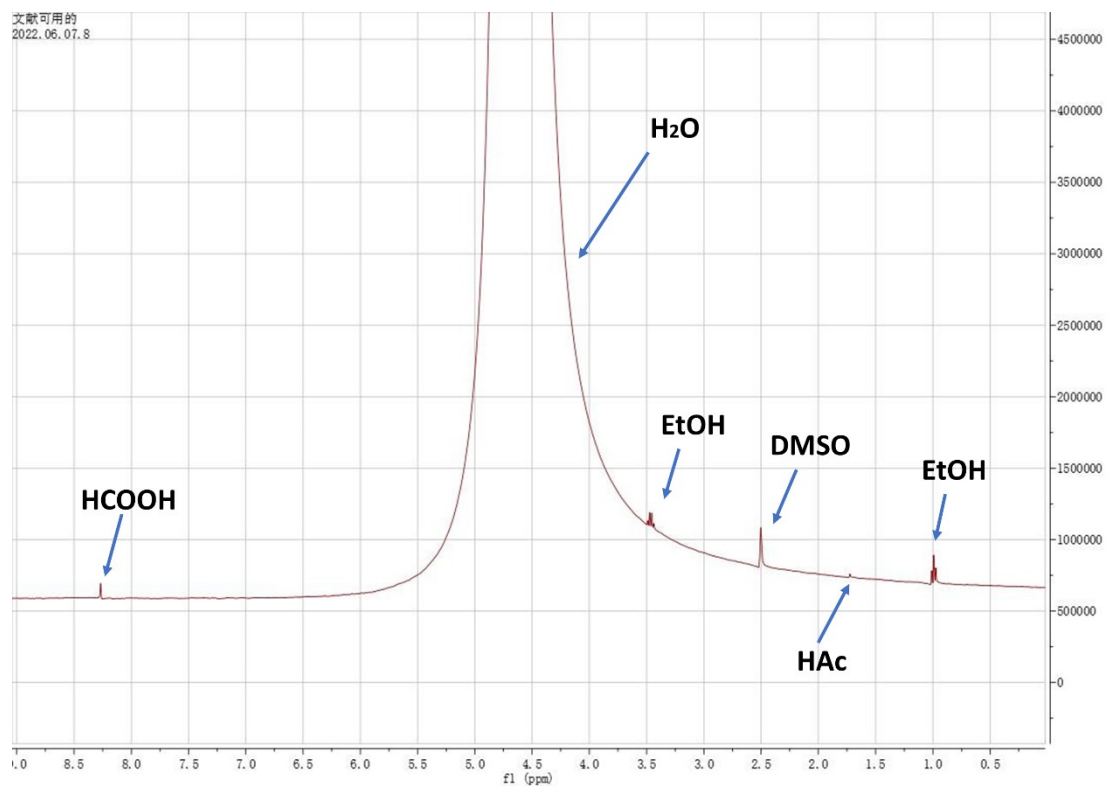


**Figure S11.** CO<sub>2</sub>RR liquid products. A representative <sup>1</sup>H-NMR spectrum of the electrolyte that collected after 2 h CO<sub>2</sub>RR

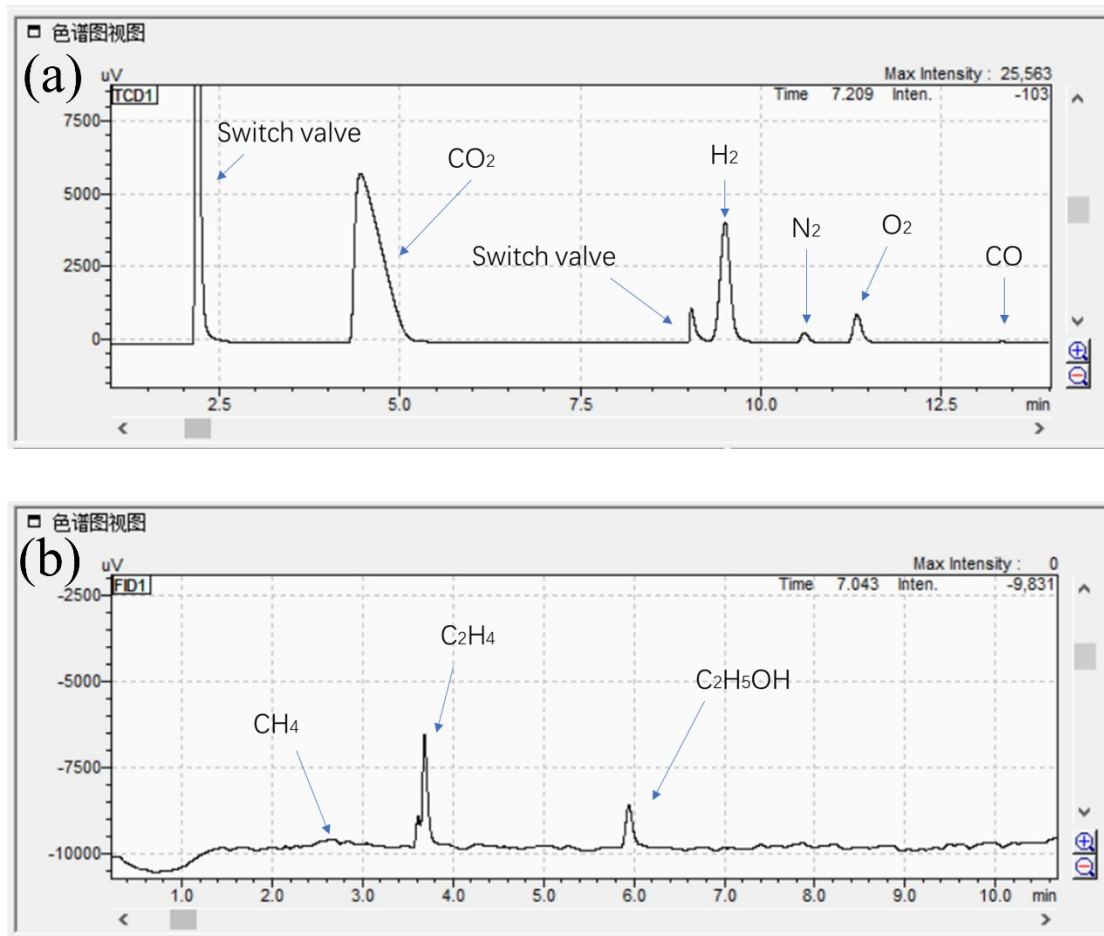


**Figure S12.**  $\text{CO}_2\text{RR}$  gas products GC spectrum with the thermal conductivity detector (TCD) and flame ionization detector (FID) detector

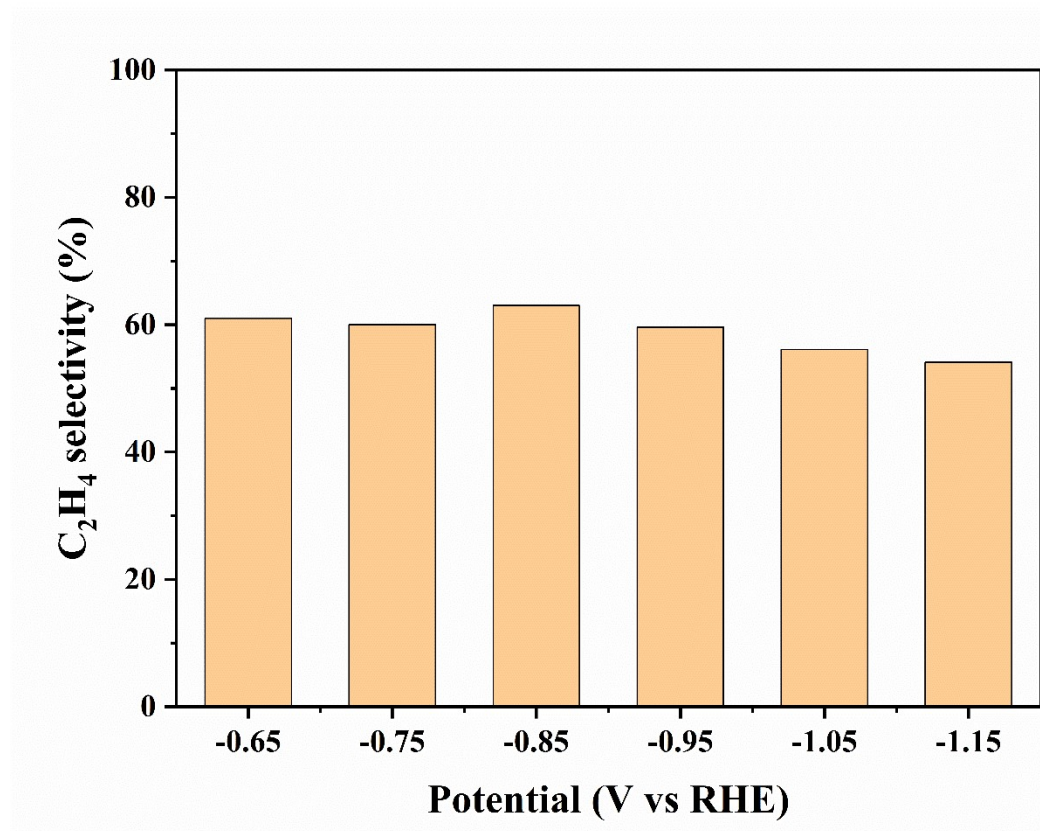


**Figure S13.** Selectivity of cathodic  $\text{CO}_2$  electroreduction to  $\text{C}_2\text{H}_4$  at different voltages in an H-type electrolyzer

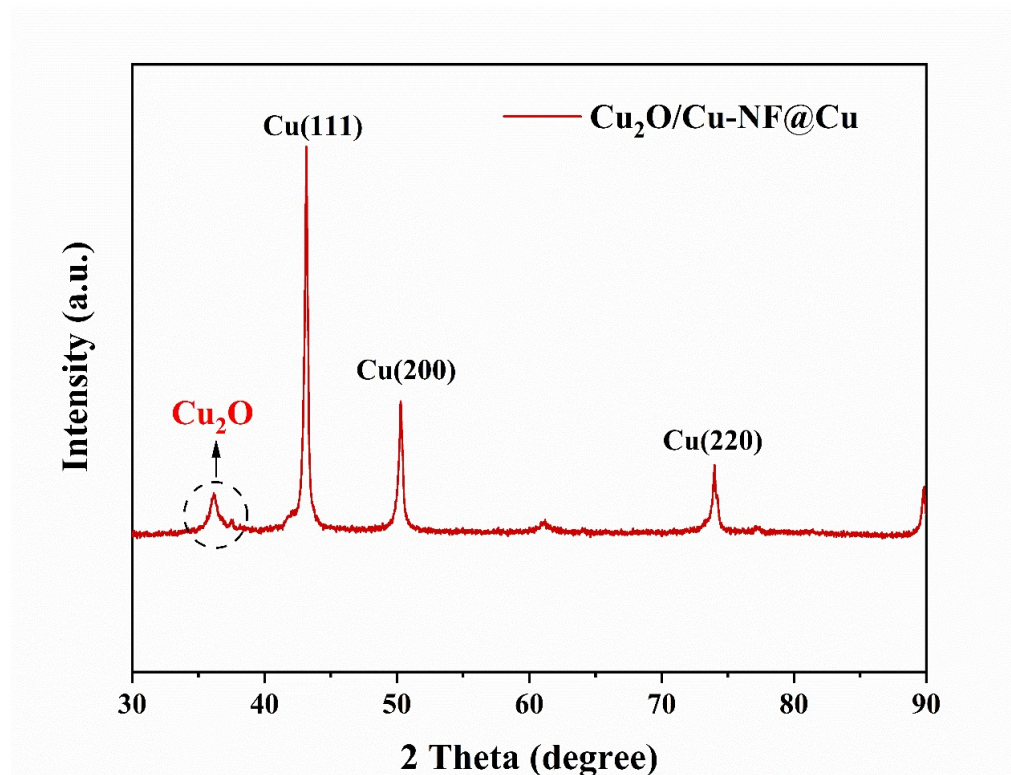


**Figure S14.** XRD profiles of  $\text{Cu}_2\text{O}/\text{Cu-NF}@\text{Cu}$  taken after 45 h  $\text{CO}_2\text{RR}$ . The  $\text{Cu}_2\text{O}$  characteristic peak still exists in  $\text{Cu}_2\text{O}/\text{Cu-NF}@\text{Cu}$

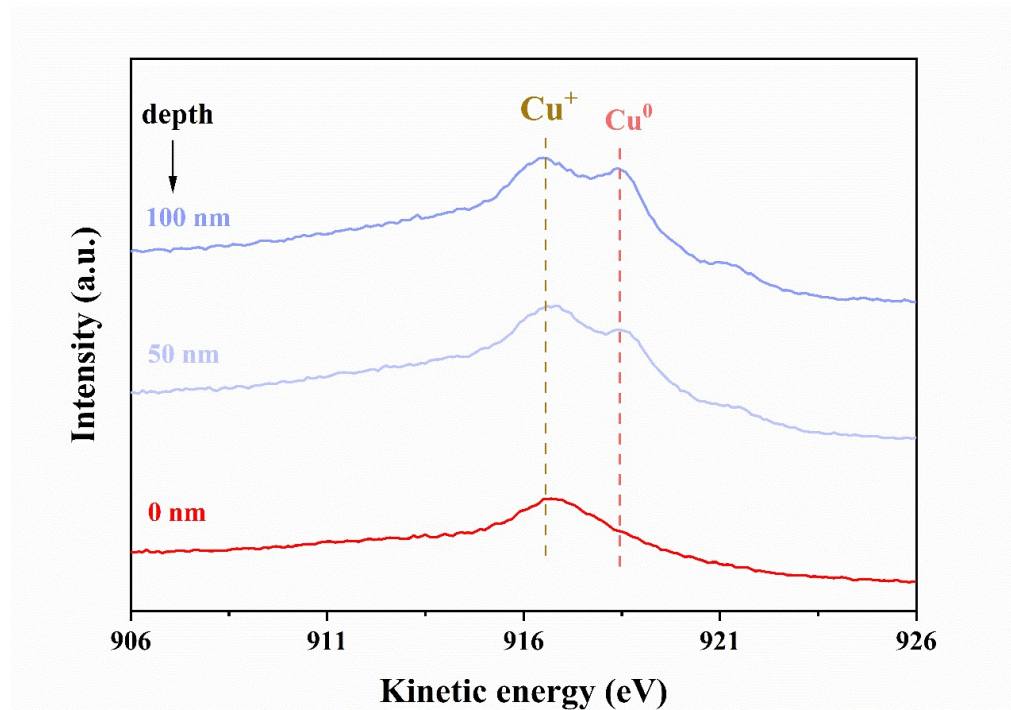


**Figure S15.** Cu LMM Auger spectra of the 45 h post-electrolysis  $\text{Cu}_2\text{O}/\text{Cu-NF}@\text{Cu}$  in  $\text{KCl}$  with respect to different  $\text{Ar}^+$  etching depths

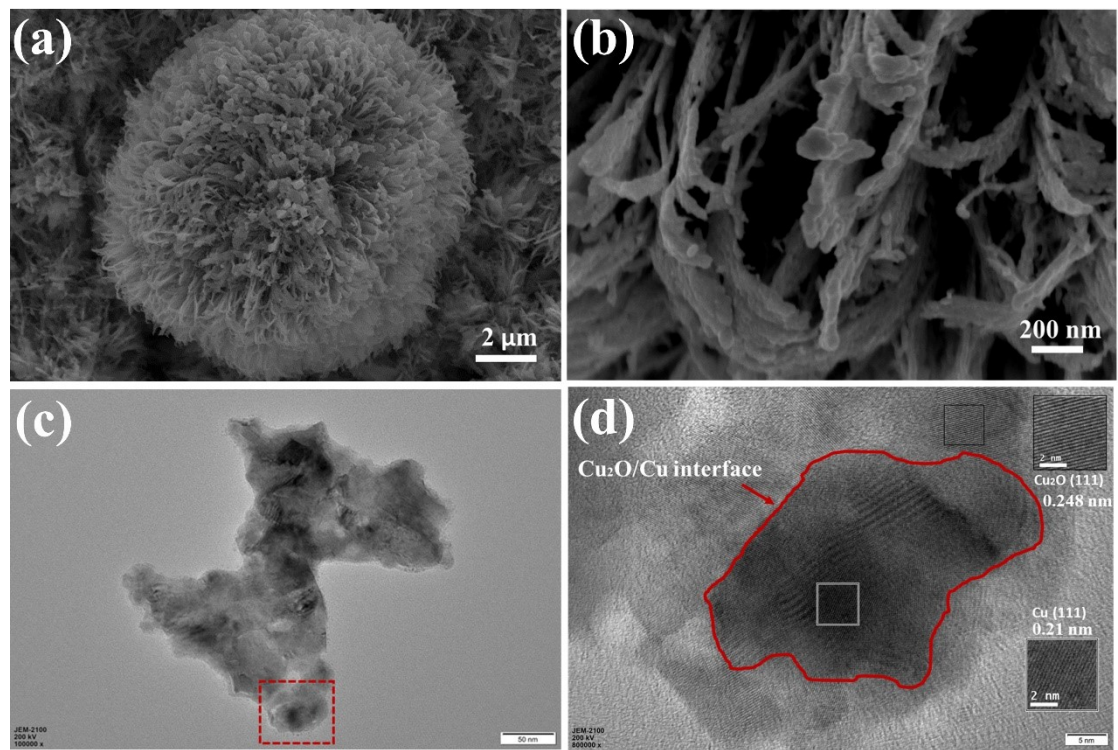


**Figure S16.** (a, b) SEM of Cu<sub>2</sub>O/Cu-NF@Cu after 45 h CO<sub>2</sub>RR. (c, d) HRTEM image of Cu<sub>2</sub>O/Cu-NF@Cu after 45 h CO<sub>2</sub>RR. The Cu<sub>2</sub>O/Cu-NF@Cu catalyst preserved a Cu<sub>2</sub>O/Cu composite structure and Cu<sub>2</sub>O/Cu interface after long-term test

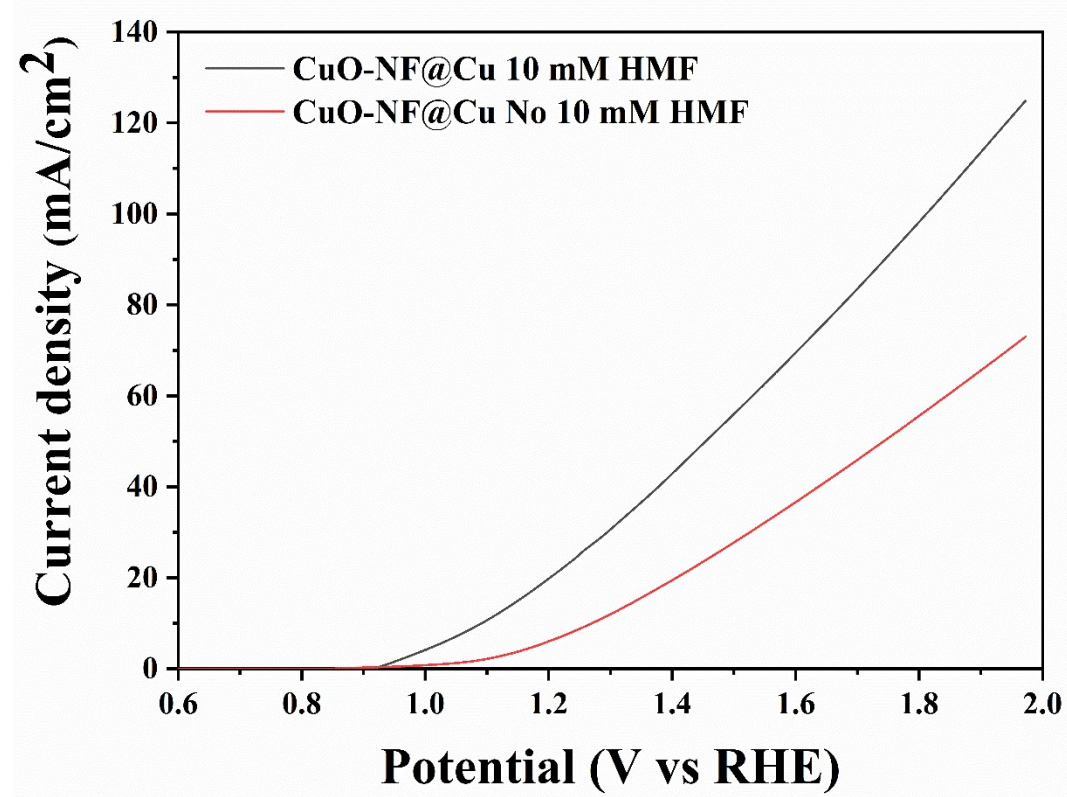


**Figure S17.** LSV curves of CuO-NF@Cu with and without 10 mM HMF

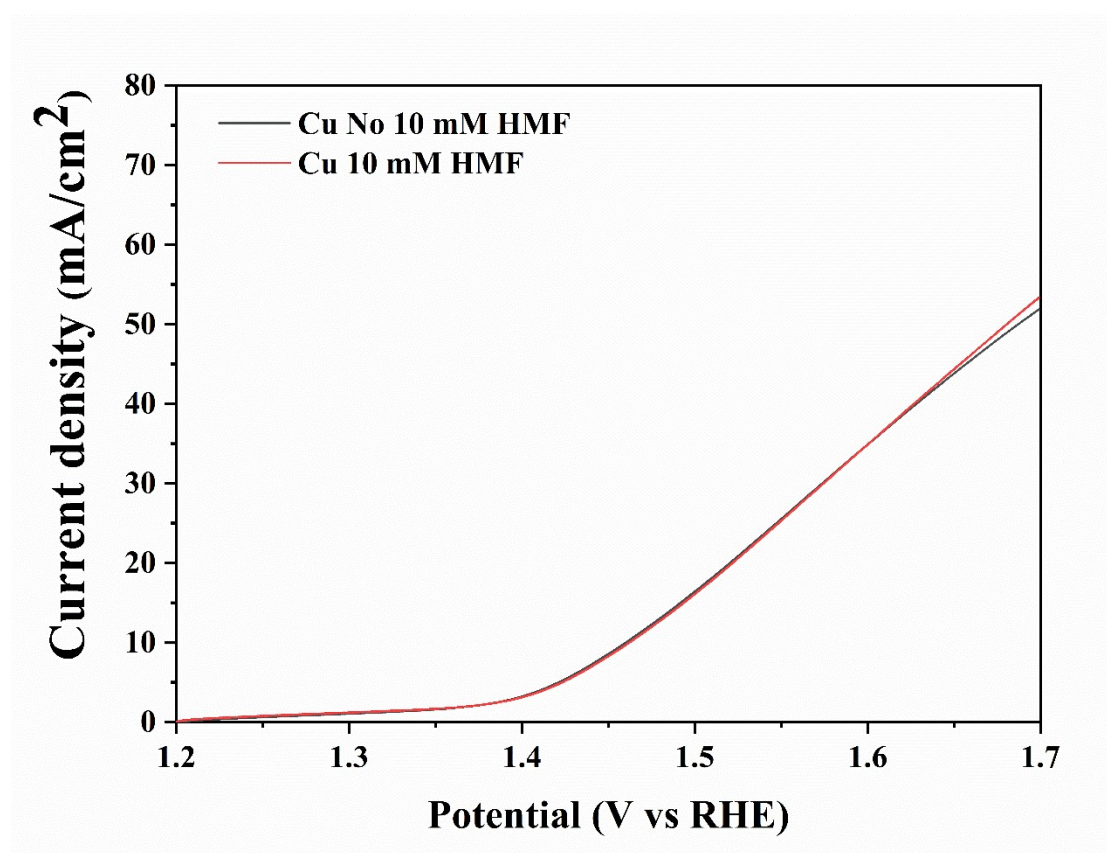


**Figure S18.** LSV curves of Cu with and without 10 mM HMF

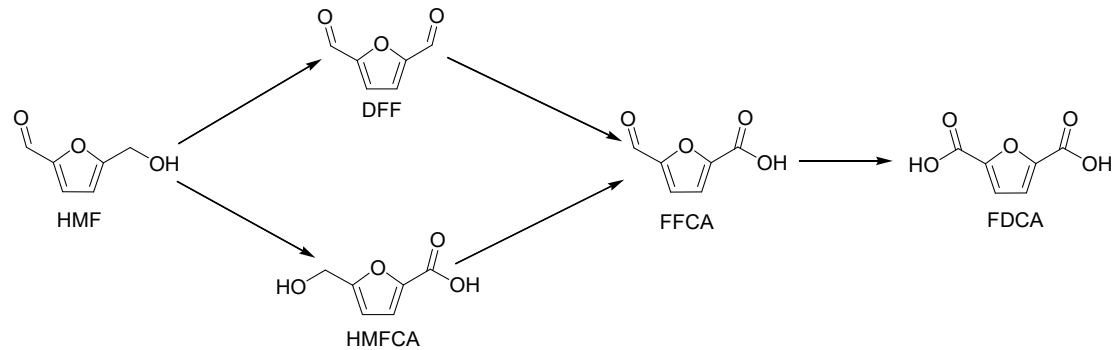


**Figure S19.** Two HMF oxidation pathways to FDCA

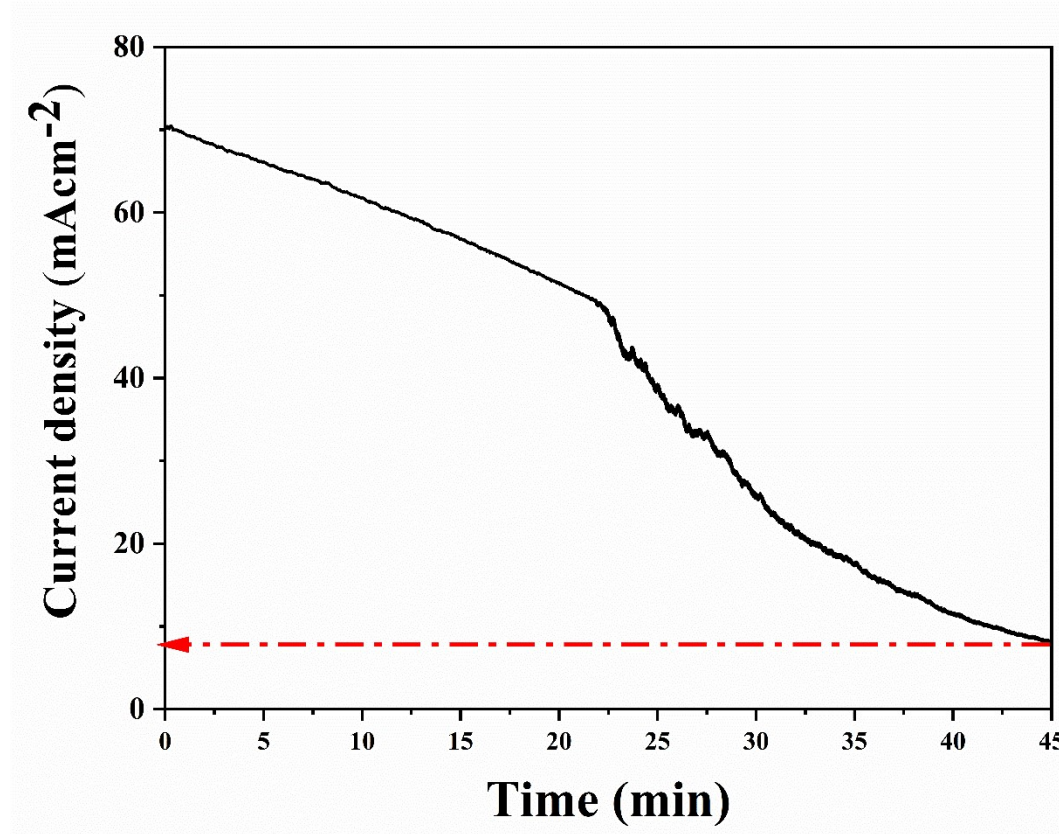


**Figure S20.** Current density in HMFOR

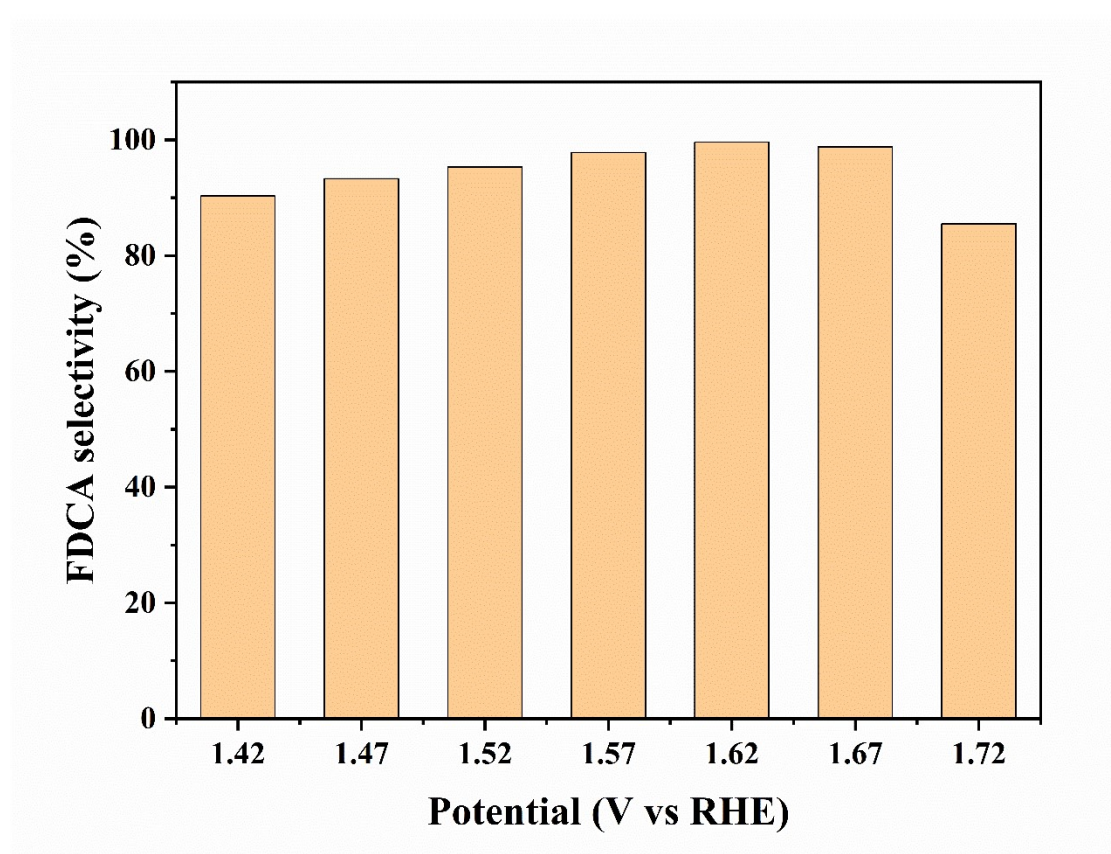


**Figure S21.** Selectivity of anodic HMF electrooxidation to FDCA at different voltages in an H-type electrolyzer

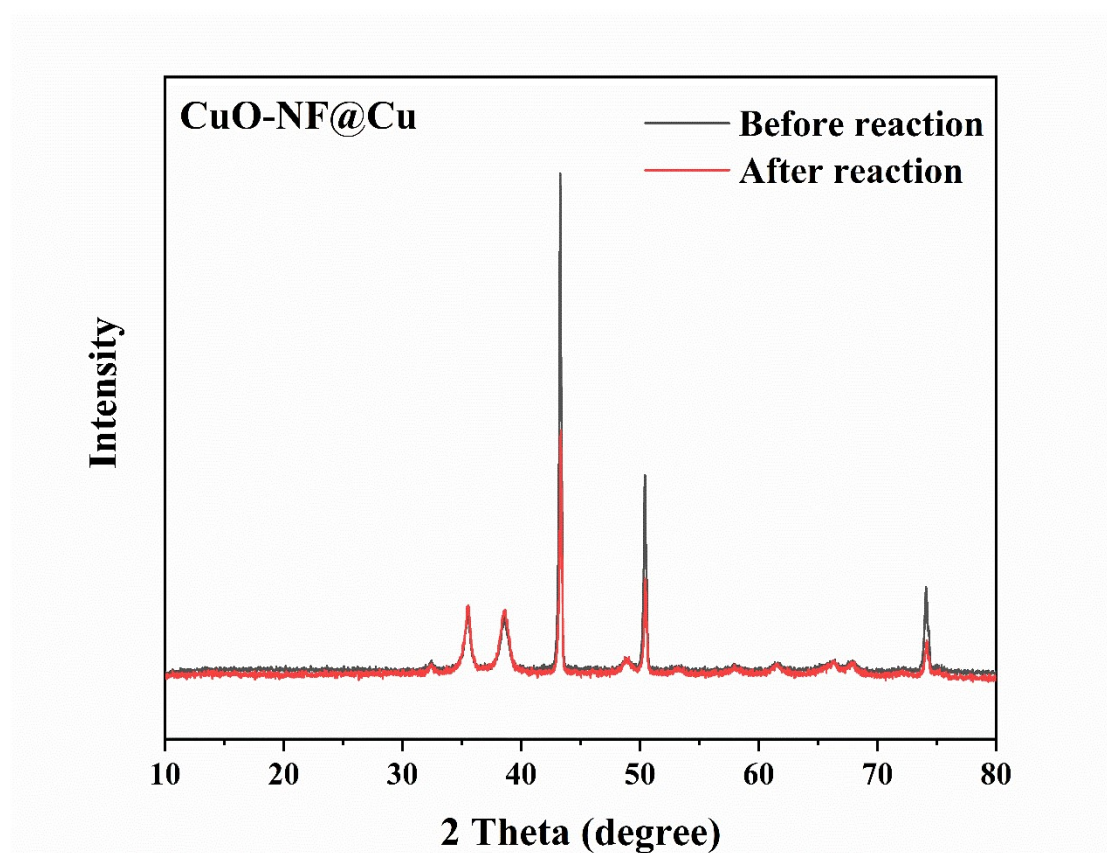


**Figure S22.** XRD patterns of CuO-NF@Cu before and after 5 recycle tests in electro-oxidation of HMF

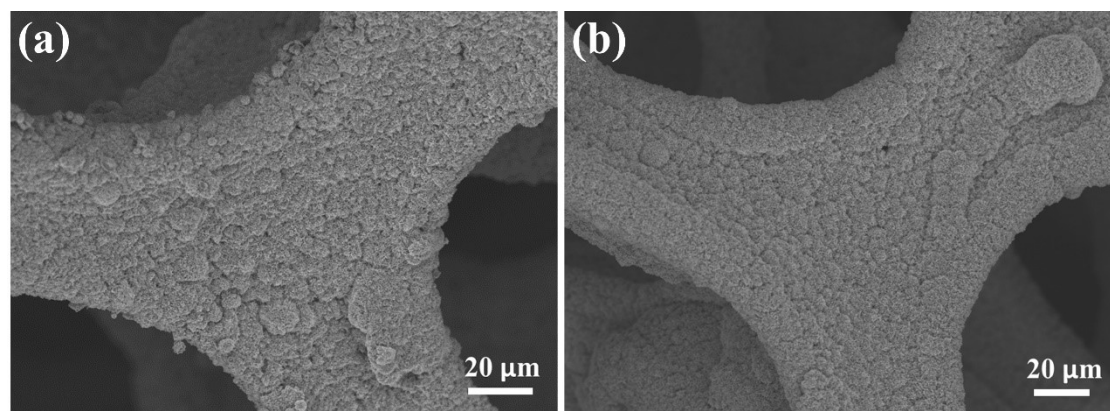


**Figure S23.** SEM imaged of CuO-NF@Cu (a) before and (b) after 5 recycle tests in electro-oxidation of HMF

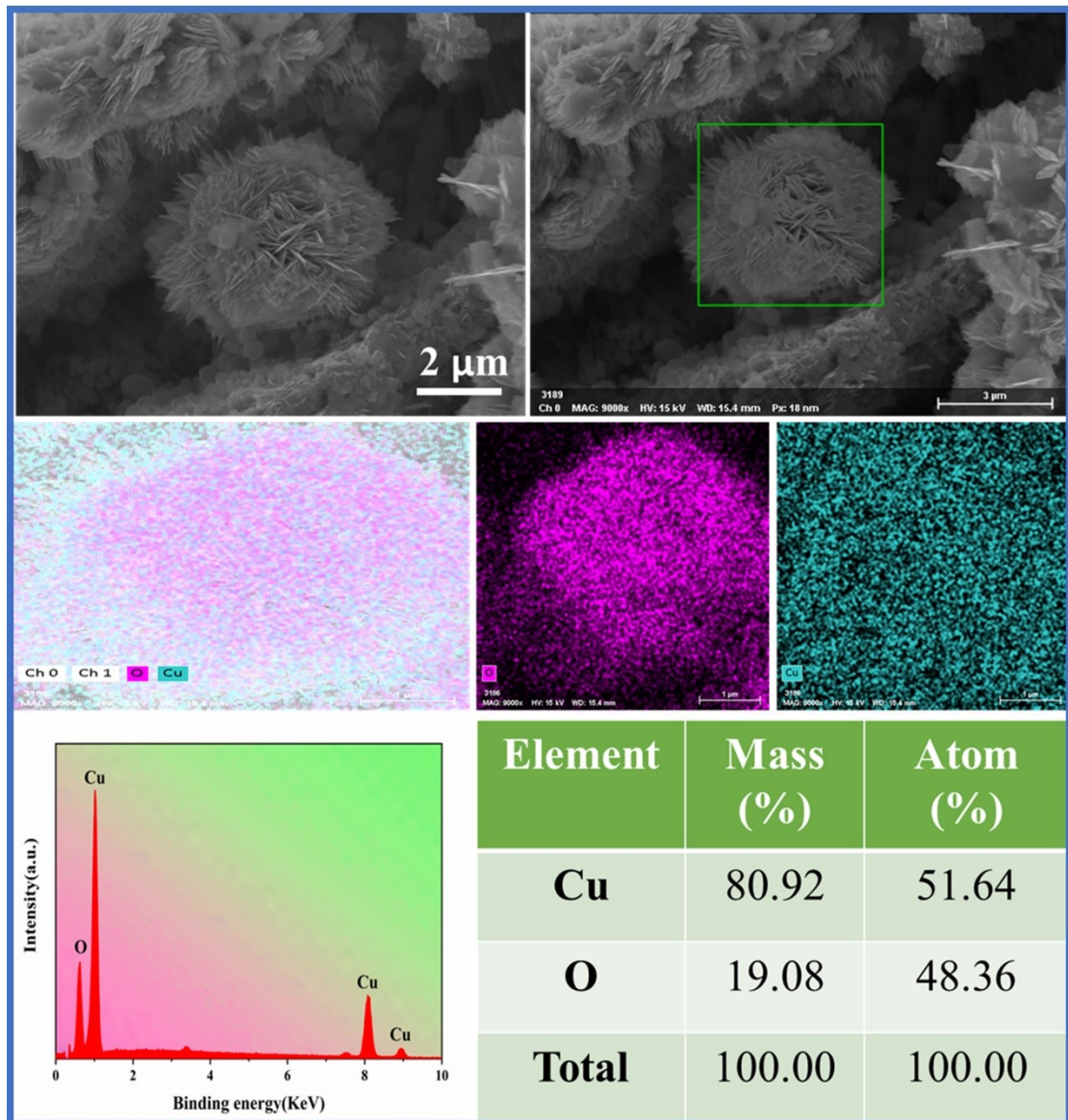


**Figure S24.** SEM images and Elemental mapping images EDS spectrum of CuO-NF@Cu after 5 recycle tests in electro-oxidation of HMF

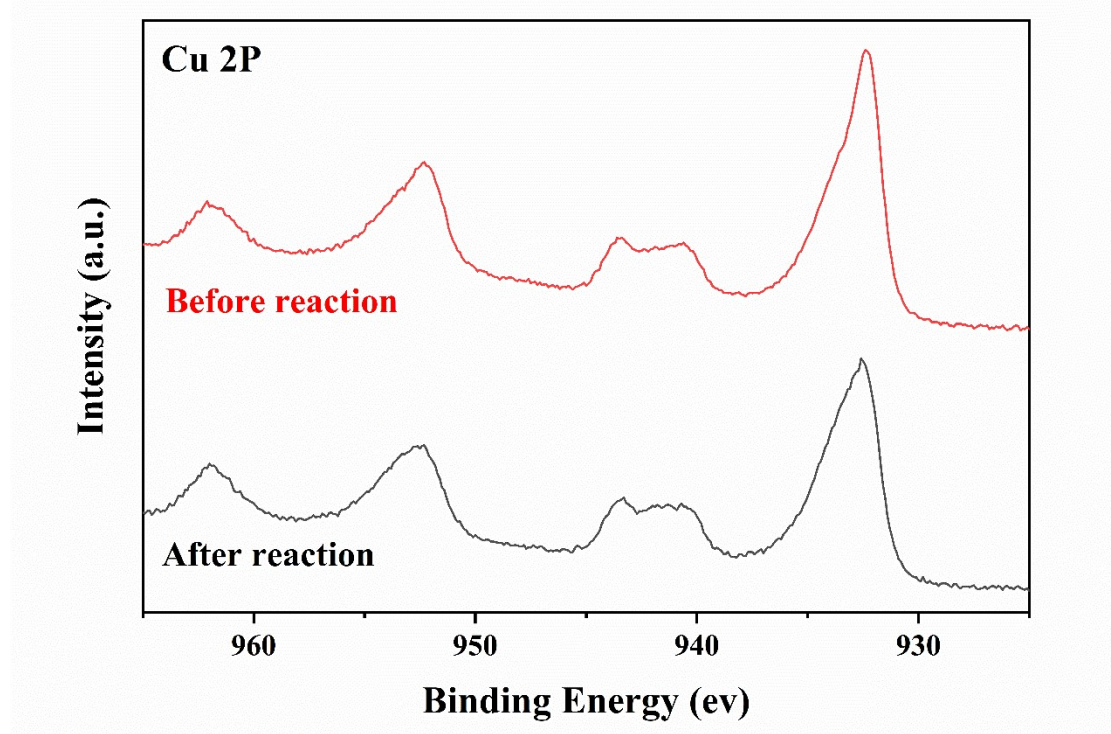


**Figure S25.** High resolution Cu2p spectra of CuO-NF@Cu before and after 5 recycle tests in electro-oxidation of HMF

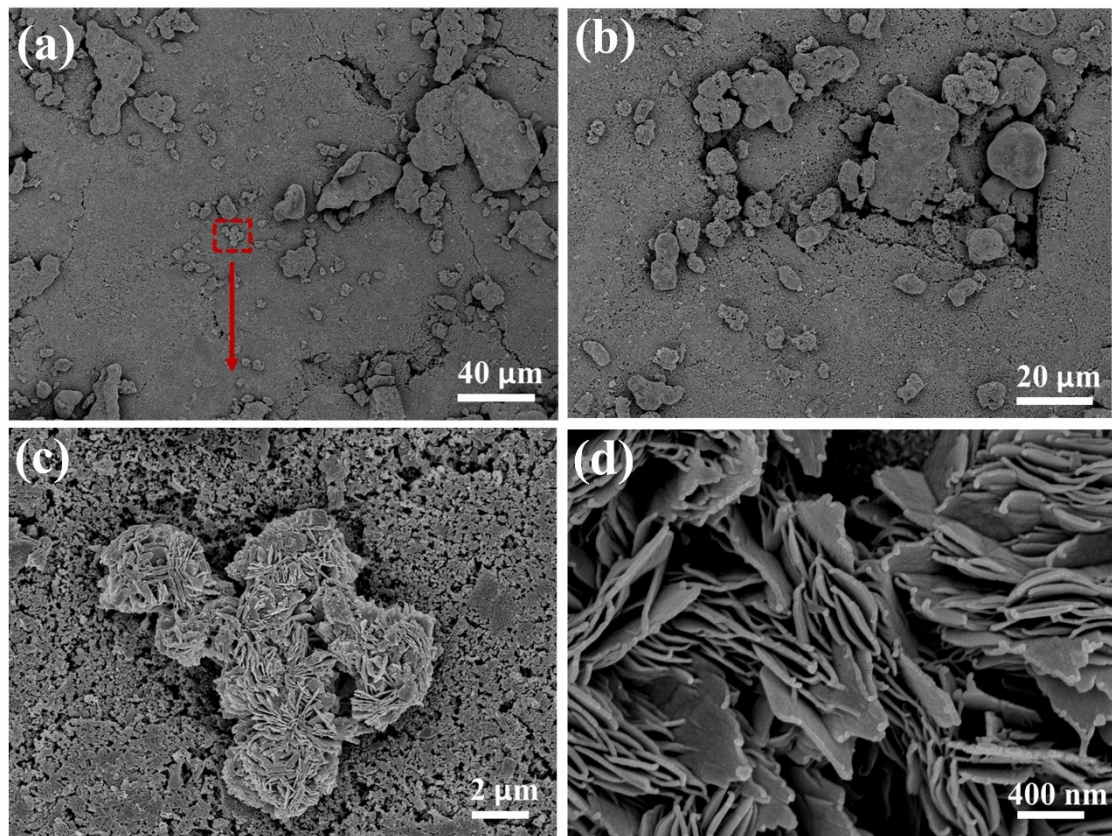


**Figure S26.** SEM images of CuO-NF@GDL at different magnification

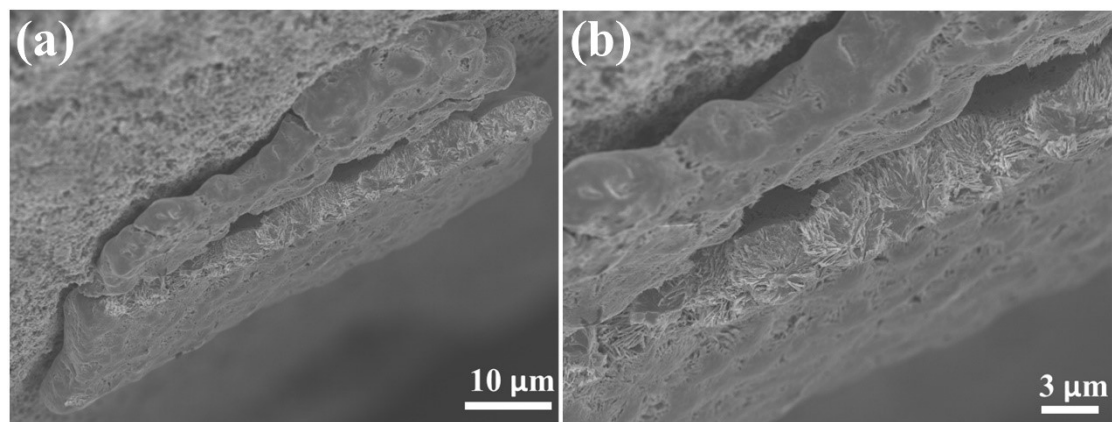


**Figure S27.** Cross-sectional SEM images of CuO-NF@GDL. The CuO-NF layer covers the surface of the microporous layer

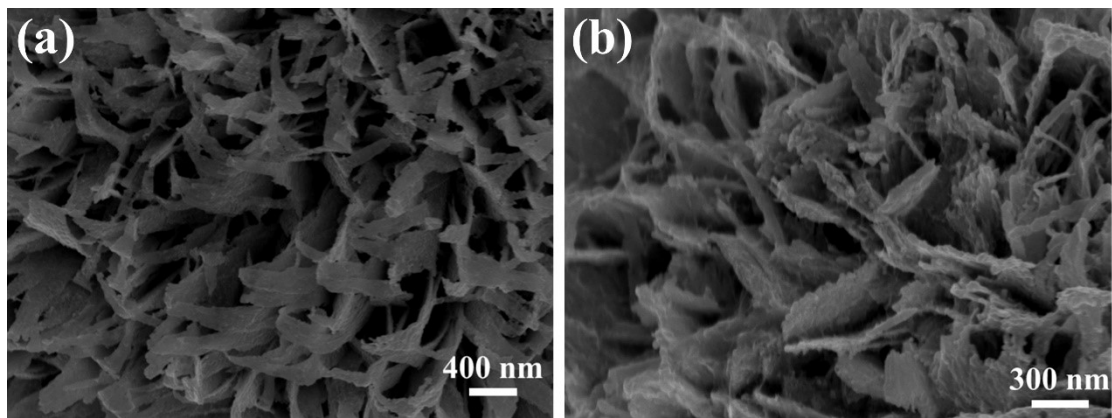


**Figure S28.** SEM images of (a) prepared fresh CuO-NF@GDL and (b) recovered Cu<sub>2</sub>O/Cu-NF@GDL after CO<sub>2</sub>RR and HMFOR. Cu<sub>2</sub>O/Cu-NF@GDL maintained the nanostructure of CuO-NF@GDL, no agglomeration in Cu<sub>2</sub>O/Cu-NF@GDL was found

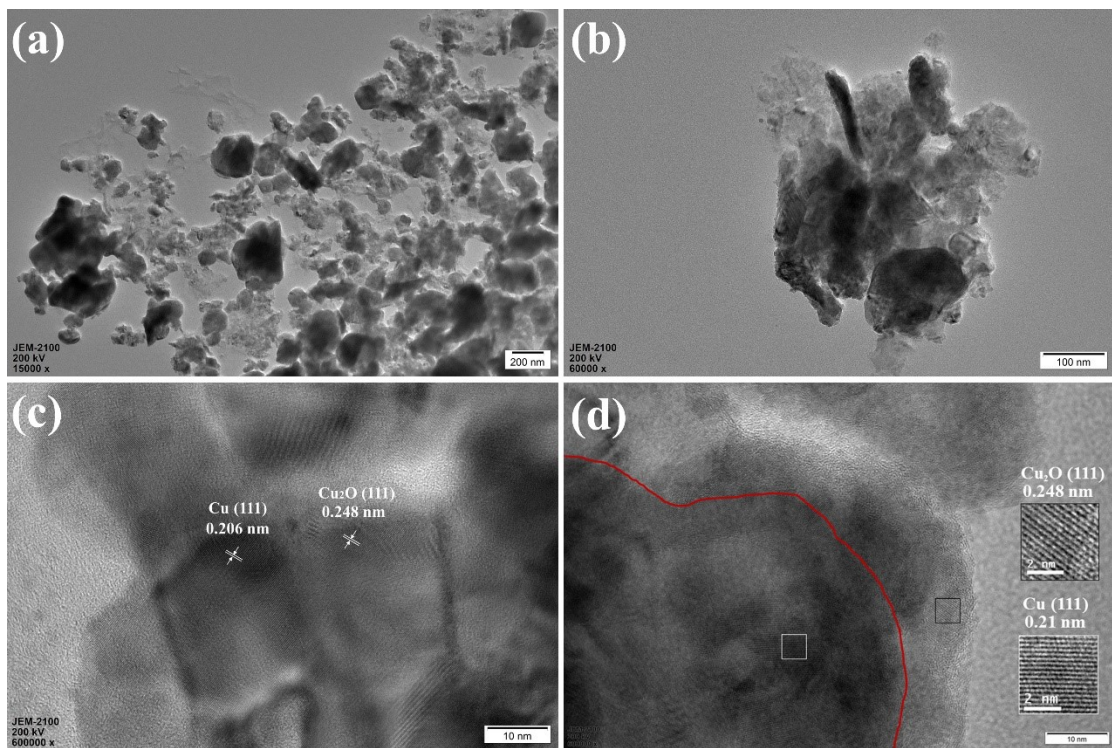


**Figure S29.** Different magnification TEM images of recovered Cu<sub>2</sub>O/Cu-NF@GDL after CO<sub>2</sub>RR and HMFOR. The nanoplates are composed of smaller nanoparticles, which have Cu<sub>2</sub>O shells and Cu cores, Cu<sub>2</sub>O/Cu interfaces can be clearly seen in HRTEM images

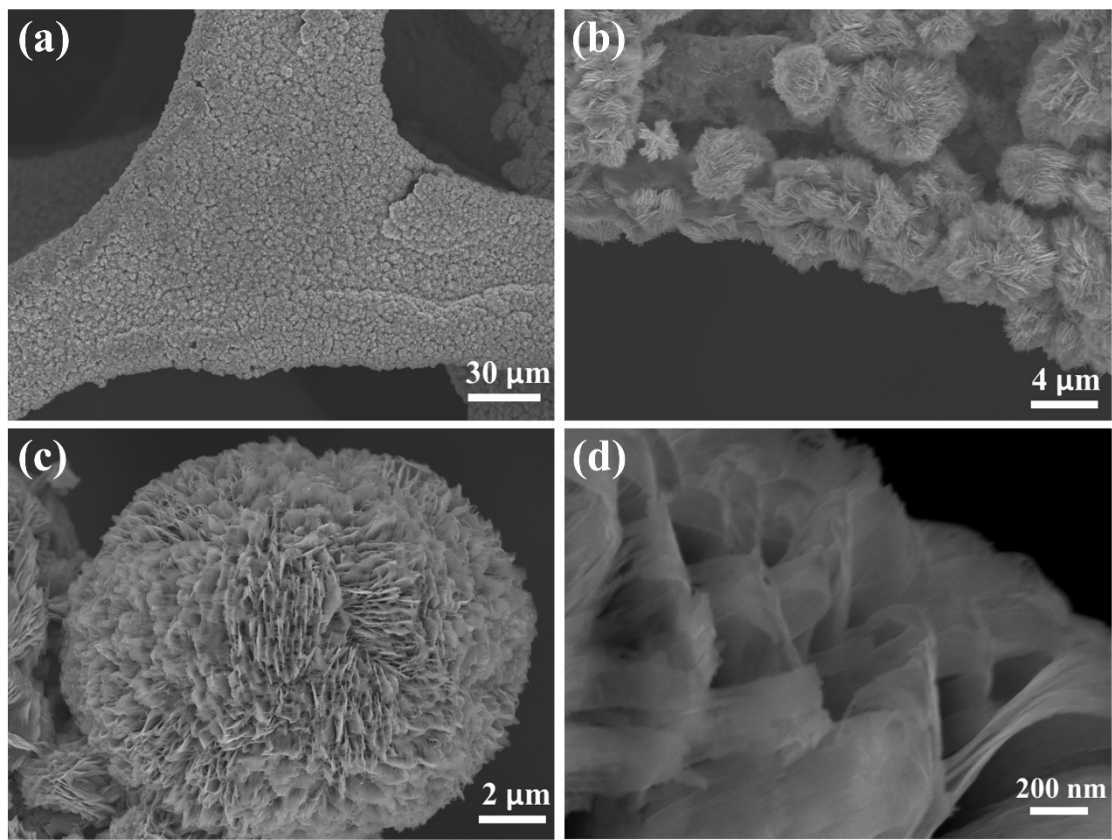


**Figure S30.** Anode CuO-NF@Cu in different magnification SEM images  
after 5 hours

**Table S1.** FEs of Cu<sub>2</sub>O/Cu-NF@Cu at different potentials in the H-cell

Potential (V)	FE(%)							
	C <sub>2</sub> H <sub>4</sub>	H <sub>2</sub>	CO	CH <sub>4</sub>	HCOOH	C <sub>2</sub> H <sub>5</sub> OH	CH <sub>3</sub> COOH	Total
-0.65	41.2	48.6	2	0	2	1	0.8	95.6
-0.75	51.1	37.9	3.1	0	2	2.5	0.5	97.1
-0.85	60.8	28.2	3.9	0	1.5	2.5	1	97.9
-0.95	70.0	16.5	5.2	1.8	1.5	3	1	99.0
-1.05	56.1	29.6	4	2.3	1.7	4.8	1	99.5
-1.15	38	45.5	2	5	1	6.1	0.5	98.1

**Table S2.** The comparison of performance among various Cu-based catalysts for CO<sub>2</sub> reduction to C<sub>2</sub>H<sub>4</sub>

Catalyst	electrolyte	Potential (V vs REH)	FE C <sub>2</sub> H <sub>4</sub> (%)	J C <sub>2</sub> H <sub>4</sub> (mA cm <sup>-2</sup> )	Run time(h)	Ref.
Cu <sub>2</sub> O/Cu-NF@Cu	0.5 M KCl	-0.95	70	73.2	45	This work
AN-Cu	0.1 M KHCO <sub>3</sub>	-1.08	38.1	7.3	40	1
Cu <sub>2</sub> O nanoparticles	0.1 M KHCO <sub>3</sub>	-1.1	57.3	11	9	2
Cu nanosheets	0.1 M K <sub>2</sub> SO <sub>4</sub>	-1.18	83.2	66.5	14	3
OBC	0.5 M KHCO <sub>3</sub>	-1	45	44.7	10	4
O <sub>2</sub> -plusma-treated Cu	0.1 M KHCO <sub>3</sub>	-0.9	60	7.2	5	5
Cu(B)-2	0.1 M KCl	-1.1	52	17.6	12	6
Star decahedron Cu	0.1 M KHCO <sub>3</sub>	-0.993	52	17.6	12	7
Cu nanocube	0.2 M KHCO <sub>3</sub>	-0.96	32.5	21	2	8

**Table S3.** Reported electrochemical oxidation of HMF to FDCA systems

Catalysts	Electrolyte/ Oxidized substrate	Potential (V vs RHE)	Charg e (C)	FDC A Yield	FDC A FE	Yield rate ( $\mu\text{mol}\cdot\text{cm}^{-2}\cdot\text{h}^{-1}$ )	Ref.
CuO- NF@Cu	0.1 M KOH/ 10 mM HMF	1.62 V	116	100%	99.3%	264.8	This work
CF- Cu(OH) <sub>2</sub>	1 M KOH/ 10 mM HMF	1.72 V	223.4	99.5%	90%	133.3	9
CoO-CoSe2	1 M KOH/ 10 mM HMF	1.43 V	89	99%	97.9%	148.5	10
NixB-NF	1 M KOH/ 10 mM HMF	1.45 V	58	98.5%	100%	197	11
MoO <sub>2</sub> -FeP	1 M KOH/ 10 mM HMF	1.42 V	116	98.6	97.8	71.4	12
t-POC/Ni- nanosheet	1 M KOH/ 10 mM HMF	1.42 V	86.7	99.9	99.7	224.1	13
NiOOH	1 M KOH/ 5 mM HMF	1.47 V	40.52	96.0%	96.0%	14.9	14
CoNW/NF	1 M KOH/ 10 mM HMF	1.47 V	300	98.7%	100%	84.47	15
NiS <sub>x</sub> /Ni <sub>2</sub> P	1 M KOH/ 10 mM HMF	1.46 V	90	98.5%	95.1%	40.1	16

## Reference

1. S. Y. Lee, H. Jung, N. K. Kim, H. S. Oh, B. K. Min and Y. J. Hwang, *J. Am. Chem. Soc.*, 2018, **140**, 8681-8689.
2. H. Jung, S. Y. Lee, C. W. Lee, M. K. Cho, D. H. Won, C. Kim, H. S. Oh, B. K. Min and Y. J. Hwang, *J Am Chem Soc*, 2019, **141**, 4624-4633.
3. B. Zhang, J. Zhang, M. Hua, Q. Wan, Z. Su, X. Tan, L. Liu, F. Zhang, G. Chen, D. Tan, X. Cheng, B. Han, L. Zheng and G. Mo, *J Am Chem Soc*, 2020, **142**, 13606-13613.
4. W. Zhang, C. Huang, Q. Xiao, L. Yu, L. Shuai, P. An, J. Zhang, M. Qiu, Z. Ren and Y. Yu, *J Am Chem Soc*, 2020, **142**, 11417-11427.
5. H. Mistry, A. S. Varela, C. S. Bonifacio, I. Zegkinoglou, I. Sinev, Y. W. Choi, K. Kisslinger, E. A. Stach, J. C. Yang, P. Strasser and B. R. Cuenya, *Nat Commun*, 2016, **7**, 12123.
6. Y. Zhou, F. Che, M. Liu, C. Zou, Z. Liang, P. De Luna, H. Yuan, J. Li, Z. Wang, H. Xie, H. Li, P. Chen, E. Bladt, R. Quintero-Bermudez, T. K. Sham, S. Bals, J. Hofkens, D. Sinton, G. Chen and E. H. Sargent, *Nat Chem*, 2018, **10**, 974-980.
7. C. Choi, T. Cheng, M. Flores Espinosa, H. Fei, X. Duan, W. A. Goddard, 3rd and Y. Huang, *Adv Mater*, 2019, **31**, e1805405.
8. K. Jiang, R. B. Sandberg, A. J. Akey, X. Liu, D. C. Bell, J. K. Nørskov, K. Chan and H. Wang, *Nature Catalysis*, 2018, **1**, 111-119.
9. X. Pang, H. Bai, H. Zhao, W. Fan and W. Shi, *ACS Catalysis*, 2022, **12**, 1545-1557.
10. X. Huang, J. Song, M. Hua, Z. Xie, S. Liu, T. Wu, G. Yang and B. Han, *Green Chemistry*, 2020, **22**, 843-849.
11. S. Barwe, J. Weidner, S. Cychy, D. M. Morales, S. Dieckhofer, D. Hiltrop, J. Masa, M. Muhler and W. Schuhmann, *Angew Chem Int Ed Engl*, 2018, **57**, 11460-11464.
12. G. Yang, Y. Jiao, H. Yan, Y. Xie, A. Wu, X. Dong, D. Guo, C. Tian and H. Fu, *Adv Mater*, 2020, **32**, e2000455.
13. D. Xu, Y. Yang, B. Zhang, Z. Yang, S. Liu and T. Mu, *ChemSusChem*, 2022, **15**, e202200822.
14. B. J. Taitt, D.-H. Nam and K.-S. Choi, *ACS Catalysis*, 2018, **9**, 660-670.
15. Z. Zhou, C. Chen, M. Gao, B. Xia and J. Zhang, *Green Chemistry*, 2019, **21**, 6699-6706.
16. B. Zhang, H. Fu and T. Mu, *Green Chemistry*, 2022, **24**, 877-884.